

1 **Response of dust emissions in southwestern North America to 21st**
2 **century trends in climate, CO₂ fertilization, and land use:**
3 **Implications for air quality**

4 Yang Li¹, Loretta J. Mickley¹, Jed O. Kaplan²

5 ¹John A. Paulson School of Engineering and Applied Sciences, Harvard University, Cambridge,
6 MA, USA

7 ²Department of Earth Sciences, The University of Hong Kong, Hong Kong, China

8 *Correspondence to:* Yang Li (yangli@seas.harvard.edu)

9

10 **Abstract.** Climate models predict a shift toward warmer and drier environments in southwestern
11 North America. The consequences of such a shift for dust mobilization and dust concentration are
12 unknown, but could have large implications for human health, given connections between dust
13 inhalation and disease. Here we link a dynamic vegetation model (LPJ-LMfire) to a chemical
14 transport model (GEOS-Chem) to assess the impacts of future changes in three factors – climate,
15 CO₂ fertilization, and land use practices – on vegetation in this region. From there we investigate
16 the impacts of changing vegetation on dust mobilization and assess the net effect on fine dust
17 concentration (defined as dust particles less than 2.5 microns in diameter) on surface air quality.
18 We find that surface temperatures in southwestern North America warm by 3.3 K and precipitation
19 decreases by nearly 40% by 2100 in the most extreme warming scenario (RCP8.5) in spring
20 (March, April, and May), the season of greatest dust emissions. Such conditions reveal an
21 increased vulnerability to drought and vegetation die-off. Enhanced CO₂ fertilization, however,
22 offsets the modeled effects of warming temperatures and rainfall deficit on vegetation in some

23 areas of the southwestern United States. Considering all three factors in RCP8.5 scenario, dust
24 concentrations decrease over Arizona and New Mexico in spring by the late 21st century due to
25 greater CO₂ fertilization and a more densely vegetated environment, which inhibits dust
26 mobilization. Along Mexico's northern border, dust concentrations increase as a result of the
27 intensification of anthropogenic land use. In contrast, when CO₂ fertilization is not considered in
28 the RCP8.5 scenario, vegetation cover declines significantly across most of the domain by 2100,
29 leading to widespread increases in fine dust concentrations, especially in southeastern New Mexico
30 (up to ~2.0 μg m⁻³ relative to the present day) and along the border between New Mexico and
31 Mexico (up to ~2.5 μg m⁻³). Our results have implications for human health, especially for the
32 health of the indigenous people who make up a large percentage of the population in this region.

33 **1 Introduction**

34 The arid and semi-arid region covering southwestern United States and northwestern
35 Mexico is characterized by large concentrations of soil-derived dust particles in the lower
36 atmosphere, especially in spring (Hand et al., 2016). By causing respiratory and cardiovascular
37 diseases, fine dust particles – i.e., those particles with diameter less than 2.5 microns – can have
38 negative effects on human health (Tong et al., 2017; Meng and Lu, 2007; Gorris et al., 2018). A
39 key question is to what extent climate change and other factors will influence future dust
40 concentrations in this region, which we define here as southwestern North America. In this study,
41 we use a suite of models to predict the future influence of three factors – climate change, increasing
42 CO₂ fertilization, and land use change – on vegetation in this region, and assess the consequences
43 for dust mobilization and dust concentrations.

44 Wind speed and vegetation cover are two key factors that determine soil erodibility and
45 dust emissions. Wind gusts mobilize dust particles from the Earth's surface, while vegetation
46 constrains dust emissions by reducing the extent of bare land and preserving soil moisture (Zender
47 et al., 2003). The high temperatures and reduced soil moisture characteristic of drought play an
48 important role in dust mobilization, since loss of vegetative cover during drought increases soil
49 erosion (Archer and Predick, 2008; Bestelmeyer et al., 2018).

50 Southwestern North America is covered by desert grassland, perennial grassland, savanna,
51 desert scrub, and grassy shrublands or woodlands (McClaran and Van Devender, 1997). In recent
52 decades, a gradual transition from grasslands to shrubland has been observed across much of this
53 region, with increased aridity, atmospheric CO₂ enrichment, and livestock grazing all possibly
54 playing a role in this trend (Bestelmeyer et al., 2018). Future climate change may further prolong
55 this transition, especially since shrubs fare better than grasses under a climate regime characterized

56 by large fluctuations in annual precipitation (Bestelmeyer et al., 2018; Edwards et al., 2019).
57 Climate models predict a warmer and drier environment in southwestern North America through
58 the 21st century, with more frequent and severe drought (Seager and Vecchi, 2010; MacDonald,
59 2010; Stahle, 2020; Prein et al., 2016; Williams et al., 2020). Such conditions would decrease
60 vegetative cover and allow for greater dust mobilization. On the other hand, elevated CO₂
61 concentrations in the future atmosphere could increase photosynthesis and decrease transpiration
62 of some vegetation species, allowing for more efficient water use and enhancing growth (Poorter
63 and Perez-Soba, 2002; Polley et al., 2013). Anthropogenic land use practices – e.g., agriculture,
64 human settlement, and urban sprawl – have changed dramatically over the southwestern North
65 America in recent decades, with Arizona and New Mexico showing decreasing cropland area and
66 northern Mexico experiencing increasing pasture area (Figure S1). Future land use practices could
67 also influence the propensity for dust mobilization by disturbing crustal biomass (e.g., Belnap and
68 Gillette, 1998).

69 Previous studies have investigated the relative importance of climate, CO₂ fertilization,
70 and/or land use in present-day and future dust emissions and concentrations, sometimes with
71 contradictory results. For example, Woodward et al., 2005 predicted a tripling of the global dust
72 burden by 2100 relative to the present day, while other studies suggested a decrease in the global
73 dust burden (e.g., Harrison et al., 2001, Mahowald and Luo, 2003 and Mahowald et al., 2006).
74 These estimates of future dust emissions depended in large part on the choice of model applied, as
75 demonstrated by Tegen et al., 2004.

76 In southwestern North America, a few recent studies examined statistical relationships
77 between observed present-day dust concentrations and meteorological conditions or leaf area index
78 (LAI). Hand et al., 2016 found that fine dust concentrations in spring in this region correlated with

79 the Pacific Decadal Oscillation (PDO), indicating the importance of large-scale climate patterns in
80 the mobilization and transport of regional fine dust. Tong et al., 2017 further determined that the
81 observed 240% increase in the frequency of windblown dust storms from 1990s to 2000s in the
82 southwestern United States was likely associated with the PDO. Similarly, Achakulwisut et al.,
83 2017 found that the 2002–2015 increase in average March fine dust concentrations in this region
84 was driven by a combination of positive PDO conditions and phase of the El Nino-Southern
85 Oscillation. More recently, Achakulwisut et al., 2018 identified the Standardized Precipitation-
86 Evapotranspiration Index as a useful indicator of present-day dust variability. Applying that metric
87 to an ensemble of future climate projections, these authors predicted increases of 26-46% in fine
88 dust concentrations over the U.S. Southwest in spring by 2100. In contrast, Pu and Ginoux, 2017
89 found that the frequency of extreme dust days decreases slightly in spring in this region due to
90 reduced extent of bare land under 21st century climate change.

91 These regional studies relied mainly on statistical models that relate local and/or large scale
92 meteorological conditions to dust emissions in southwestern North America. Pu and Ginoux, 2017
93 also considered changing LAI in their model, but these dust-LAI relationships were derived from
94 a relatively sparse dataset, casting some uncertainty on the results (Achakulwisut et al., 2018). In
95 this study, we investigate the effects of climate change, increasing CO₂ fertilization, and future
96 land use practices on vegetation in southwestern North America, and we examine the response of
97 dust mobilization due to these changes in vegetation. With regard to climate, we examine whether
98 a shift to warmer, drier conditions by 2100 enhances dust mobilization in this region by reducing
99 vegetation cover and exposing bare land. To that end, we couple the LPJ-LMfire dynamic
100 vegetation model to the chemical transport model GEOS-Chem to study vegetation dynamics and
101 dust mobilization under different conditions and climate scenarios, allowing consideration of

102 several factors driving future dust mobilization in the southwestern North America. We focus on
103 fine dust particles in springtime (March, April, and May), because it is the season of highest dust
104 concentrations in the southwestern U.S. (Hand et al., 2017). Given the deleterious impacts of
105 airborne dust on human health, our dust projections under different climate scenarios have value
106 for understanding the full array of potential consequences of anthropogenic climate change.

107

108 **2 Methods**

109 We examine dust mobilization in southwestern North America, here defined as 25°N –
110 37°N, 100°W – 115°W (Figure 1), during the late-21st century under scenarios of future climate
111 and land use based on two Representative Concentration Pathways (RCPs). RCP4.5 and RCP8.5
112 capture two possible climate trajectories over the 21st century, beginning in 2006. RCP4.5
113 represents a scenario of moderate future climate change with gradual reduction in greenhouse gas
114 (GHG) emissions after 2050 and a radiative forcing at 2100 relative to pre-industrial values of +4.5
115 W m⁻², while RCP8.5 represents a more extreme scenario with continued increases in GHGs
116 throughout the 21st century and a radiative forcing of +8.5 W m⁻² at 2100. For each RCP, we
117 investigate the changes in vegetation for three cases: 1) an all-factor case that includes changes in
118 climate, land use, and CO₂ fertilization; 2) a fixed-CO₂ case that includes changes in only climate
119 and land use; and 3) a fixed-land use case that includes changes in only climate and CO₂
120 fertilization.

121 We use LPJ-LMfire, a dynamic global vegetation model, to estimate changes in vegetation
122 under future conditions (Pfeiffer et al., 2013). Meteorology to drive LPJ-LMfire is taken from the
123 Goddard Institute for Space Studies (GISS) climate model (Nazarenko et al., 2015). Using the
124 GEOS-Chem emission component (HEMCO), we then calculate dust emissions based on the LPJ-

125 generated vegetation area index (VAI) for all scenarios. We apply the resulting dust emissions to
126 the global chemical transport model GEOS-Chem to simulate the distribution of fine dust across
127 the southwestern North America.

128

129 **2.1 GISS Model E**

130 Present-day and future meteorological fields for RCP4.5 and RCP8.5 are simulated by the
131 GISS Model E climate model (Nazarenko et al., 2015), configured for Phase 5 of the Coupled
132 Model Intercomparison Project (CMIP5; <https://esgf-node.llnl.gov/search/cmip5/>, last accessed on
133 17 July 2020). The simulations cover the years 1801 to 2100 at a spatial resolution of 2° latitude x
134 2.5° longitude. Changes in climate in the GISS model are driven by increasing greenhouse gases.
135 In RCP4.5, CO₂ concentrations increase to 550 ppm by 2100; in RCP8.5 the CO₂ increases to 1960
136 ppm ((Meinshausen et al., 2011).

137 Under RCP4.5, the GISS model predicts a slight increase of 0.45 K in springtime mean
138 surface temperatures and an increase in mean precipitation by ~17% over the southwestern North
139 America by the 2100 time slice (2095-2099), relative to the present day (2011-2015). In contrast,
140 under RCP8.5, the 5-year mean springtime temperature increases significantly by 3.29 K by 2100
141 and mean precipitation decreases by ~39%. The spatial distributions of the changes in temperature
142 and precipitation by 2100 under RCP8.5 are presented in the Supplement (Figure S2). In addition,
143 lightning strike densities decrease by ~0.006 strikes km⁻² d⁻¹ over Arizona in RCP4.5, but increase
144 by the same magnitude in this region in RCP8.5 (Li et al., 2020). Lightning strikes play a major
145 role for wildfire ignition in this region, while wildfires may influence landscape succession (e.g.,
146 Bodner and Robles, 2017). Finally, future surface wind speeds do not change significantly under
147 RCP4.5, but increase slightly by ~4% across southwestern North America under RCP8.5 by 2100

148 (not shown). The increasing winds in RCP8.5 will influence the spread of fires in our study, but
149 will not affect the simulated dust fluxes directly, as described in more detail below. Compared to
150 those from other climate models, the GISS projections of climate change in southwestern North
151 America are conservative (Ahlström et al., 2012; Sheffield et al., 2013), implying that our
152 predictions of the impact of climate change on dust mobilization may also be conservative.

153 In our study, we do not specifically track drought frequency under future climate, as the
154 definition of drought is elusive (Andreadis et al., 2005; Van Loon et al., 2016). Nonetheless, the
155 meteorological conditions predicted in the RCP8.5 scenario for 2100 align with previous studies
156 projecting increased risk of drought in this region (e.g., Williams et al., 2020), and as we shall see,
157 such conditions, in the absence of CO₂ fertilization, result in decreased vegetation and greater dust
158 mobilization.

159 **2.2 LPJ-LMfire**

160 LPJ-LMfire is a dynamic vegetation model that includes a process-based representation of
161 fire (Pfeiffer et al., 2013). Input to LPJ-LMfire includes meteorological variables, soil
162 characteristics, land use, and atmospheric CO₂ concentrations, and the model then simulates the
163 corresponding vegetation structure, biogeochemical cycling, and wildfire at a spatial resolution of
164 0.5° latitude x 0.5° longitude. Here “vegetation structure” refers to vegetation types and the spatial
165 patterns in landscapes.

166 More specifically, LPJ-LMfire simulates the impacts of photosynthesis, evapotranspiration,
167 and soil water dynamics on vegetation structure and the population densities of different plants
168 functional types (PFTs). The model considers the coupling of different ecosystem processes, such
169 as the interactions between CO₂ fertilization, evapotranspiration, and temperature as well as the
170 competition among different PFTs for water resources (e.g., precipitation, surface runoff, and

171 drainage). The different PFTs in LPJ-LMfire respond differently to changing CO₂, with CO₂
172 enrichment preferentially stimulating photosynthesis in woody vegetation and C₃ grasses
173 compared to C₄ grasses (Polley et al., 2013). Wildfire in LPJ-LMfire depends on lightning ignition,
174 and the simulation considers multiday burning, coalescence of fires, and the spread rates of
175 different vegetation types. The effects of changing fire activity on vegetation cover are then taken
176 into account (Pfeiffer et al., 2013; Sitch et al., 2003; Chaste et al., 2019). Li et al., 2020 predicted
177 a ~50% increase in fire-season area burned by 2100 under scenarios of both moderate and intense
178 future climate change over the western United States. However, the effects of changing fire on
179 vegetation cover are insignificant in the grass and bare ground-dominated ecosystems of the desert
180 Southwest, where the low biomass fuels cannot support extensive spread of fires.

181 For this study we follow Li et al., 2020, in linking meteorology from GISS-E2-R to LPJ-
182 LMfire in order to capture the effects of climate change on vegetation. Meteorological fields from
183 the GISS model include monthly mean surface temperature, diurnal temperature range, total
184 monthly precipitation, number of days in the month with precipitation greater than 0.1 mm,
185 monthly mean total cloud cover fraction, and monthly mean surface wind speed. Monthly mean
186 lightning strike density, calculated using the GISS convective mass flux and the empirical
187 parameterization of Magi, 2015, is also applied to LPJ-LMfire. To downscale the 2° x 2.5° GISS
188 meteorology to finer resolution for LPJ-LMfire, we calculate the 2010-2100 monthly anomalies
189 relative to the average over the 1961-1990 period, and then add these anomalies to an
190 observationally based climatology (Pfeiffer et al., 2013). LPJ-LMfire then simulates the response
191 of natural vegetation to the 21st century trends in these meteorological fields and to increasing CO₂.
192 We apply the same changes in CO₂ concentrations as those applied to the GISS model.

193 We overlay the changes in natural land cover with future land use scenarios from CMIP5

194 (Hurtt et al., 2011; <http://tntcat.iiasa.ac.at/RcpDb/>, last accessed on 17 July 2020). Such land use
195 includes agriculture, human settlement, and urban sprawl, all of which result in habitat loss and
196 the fragmentation of forested landscapes. Present-day land use prepared for CMIP5 is taken from
197 the HYDE database v3.1 (Goldewijk, 2001; Goldewijk et al., 2010), which in turn is based on
198 array of sources, including satellite observations and government statistics. In our simulations, fire
199 is not allowed to occur on cropland and rangeland, so we do consider some land management. On
200 the other hand, our model does not account for the density of livestock on rangeland, which when
201 mismanaged, can lead to reduction of vegetation cover and enhanced dust emissions. In RCP8.5,
202 the extent of cropland and pasture cover increases by ~30% in Mexico but decreases by 10-20%
203 over areas along Mexico's northern border in the U.S. (Hurtt et al., 2011). Only minor changes in
204 land use practices by 2100 are predicted under RCP4.5 (Hurtt et al., 2011).

205 We perform global simulations with LPJ-LMfire on a $0.5^\circ \times 0.5^\circ$ grid for the two RCPs
206 from 2006-2100, and analyze results over southwestern North America, where dust emissions are
207 especially high. For each RCP we consider the effects of changing climate on land cover, as well
208 as the influence of anthropogenic land use change and CO_2 fertilization. The LPJ-LMfire
209 simulations yield monthly timeseries of the leaf area indices (LAI) and fractional vegetation cover
210 (σ_v) for nine plant functional types (PFTs): tropical broadleaf evergreen, tropical broadleaf
211 raingreen, temperate needleleaf evergreen, temperate broadleaf evergreen, temperate broadleaf
212 summergreen, boreal needleleaf evergreen, and boreal summergreen trees, as well as C_3 and C_4
213 grasses. We further discuss the LPJ-LMfire present-day land cover in the Supplement.

214 **2.3 VAI calculation**

215 Vegetation constrains dust emissions in two ways: 1) by competing with bare ground as a
216 sink for atmospheric momentum, which results in less drag on erodible soil (Nicholson et al., 1998;

217 Raupach, 1994); and 2) by enhancing soil moisture through plant shade and root systems (Hillel,
 218 1982). Here we implement the dust entrainment and deposition (DEAD) scheme of Zender et al.,
 219 2003 to compute a size-segregated dust flux, which includes entrainment thresholds for saltation,
 220 moisture inhibition, drag partitioning, and saltation feedback. The scheme assumes that vegetation
 221 suppresses dust mobilization by linearly reducing the fraction of bare soil exposed in each grid
 222 cell:

$$223 \quad A_m = (1 - A_l - A_w)(1 - A_s)(1 - A_v) \quad (1),$$

224 where A_l is the fraction of land covered by lakes, A_w is the fraction covered by wetlands, A_s is the
 225 fraction covered by snow, and A_v is the fraction covered by vegetation.

226 For this study, we use VAI as a metric to represent vegetation because it includes not only
 227 leaves but also stems and branches, all of which constrain dust emission. VAI is used to calculate
 228 A_v in equation (1) through

$$229 \quad A_v = \min [1.0, \min(VAI, VAI_t) / VAI_t] \quad (2),$$

230 where VAI_t is the threshold for complete suppression of dust emissions, set here to $0.3 \text{ m}^2 \text{ m}^{-2}$
 231 (Zender et al., 2003; Mahowald et al., 1999).

232 To compute the dust fluxes, we need to convert LAI from LPJ-LMfire to VAI. VAI is
 233 generally defined as the sum of LAI plus stem area index (SAI). Assuming immediate removal of
 234 all dead leaves, the fractional vegetation cover, σ_v , can be used to represent SAI for the different
 235 PFTs (Zeng et al., 2002). Given that the threshold VAI_t for no dust emission is relatively low (0.3
 236 $\text{m}^2 \text{ m}^{-2}$), leaf area dominates stem area in the suppression of dust mobilization in the model. In
 237 areas where LAI is greater than SAI, we therefore assume that SAI does not play a role in
 238 controlling dust emissions, and we set LAI equivalent to VAI. We also assume that C_3 and C_4
 239 grasses have zero stem area to avoid overestimating VAI during the winter and early spring when

240 such grasses are dead. Based on the method of Zeng et al., 2002, with modifications, we calculate
241 VAI in each grid cell as

$$242 \quad VAI = \max (\sum_{PFT=1}^9 LAI, \sum_{PFT=1}^7 \sigma_v) \quad (3)$$

243 where LAI is for the nine PFTs from LPJ-LMfire, and σ_v is for just seven PFTs, with σ_v for C₃
244 and C₄ grasses not considered. Of the nine PFTs, temperate needleleaf evergreen, temperate
245 broadleaf evergreen, temperate broadleaf summergreen, and C₃ grasses dominate the region, with
246 temperate needleleaf evergreen having the highest LAI in spring. This mix of vegetation type is
247 consistent with observations (e.g., (McClaran and Van Devender, 1997).

248 **2.4 Calculation of dust emissions**

249 Dust emissions are calculated offline in the DEAD dust mobilization module within the
250 Harvard-NASA Emissions Component (HEMCO). We feed into the DEAD module both the VAI
251 generated by LPJ-LMfire and meteorological fields from the Modern-Era Retrospective analysis
252 for Research and Applications (MERRA-2) at a spatial resolution of 0.5° latitude x 0.625°
253 longitude (Gelaro et al., 2017). Dust emission is nonlinear with surface windspeed. Following
254 Ridley et al., 2013, we characterize subgrid-scale surface winds as a Weibull probability
255 distribution, which allows saltation even when the grid-scale wind conditions are below some
256 specified threshold speed. The scheme assumes that the vertical flux of dust is proportional to the
257 horizontal saltation flux, which in turn depends on surface friction velocity and the aerodynamic
258 roughness length Z_0 . As recommended by Zender et al., 2003, and consistent with Fairlie et al.,
259 2007 and Ridley et al., 2013, we uniformly set Z_0 to 100 μm across all dust candidate grid cells.

260 With this model setup, we calculate hourly dust emissions for two five-year time slices for
261 each RCP and condition, covering the present day (2011-2015) and the late-21st century (2095-
262 2099). Dust emissions are generated for four size bins with radii of 0.1 – 1.0 μm , 1.0 – 1.8 μm , 1.8

263 – 3.0 μm , 3.0 – 6.0 μm . These dust emissions are then applied to GEOS-Chem. Calculated present-
264 day VAI and fine dust emissions are shown in Figure S3, and we compare modeled VAI with that
265 observed in Figures S4 and S5.

266

267 **2.5 GEOS-Chem**

268 We use the aerosol-only version of the GEOS-Chem chemical transport model (version
269 12.0.1; <http://acmg.seas.harvard.edu/geos/>). For computational efficiency, we apply monthly mean
270 oxidants archived from a full-chemistry simulation (Park et al., 2004). To isolate the effect of
271 changing dust mobilization on air quality over the southwestern North America, we use present-
272 day MERRA-2 reanalysis meteorology from NASA/GMAO (Gelaro et al., 2017) for both the
273 present-day and future GEOS-Chem simulations. In other words, we neglect the direct effects of
274 future changes in wind speeds on dust mobilization, allowing us to focus instead on the indirect
275 effects of changing vegetation on dust. For each time slice, we first carry out a global GEOS-Chem
276 simulation at 4° latitude x 5° longitude spatial resolution, and then downscale to 0.5° x 0.625° via
277 grid nesting over the North America domain. In this study, we focus only on dust particles in the
278 finest size bin (i.e., with radii of 0.1 – 1.0 μm), as these are most deleterious to human health. We
279 compare modeled fine dust concentrations over southwestern North America for the present-day
280 against observations from the IMPROVE network in Figures S6-S7.

281

282 **3 Results**

283 **3.1 Spatial shifts in springtime vegetation area index**

284 Figure 1 shows large changes in the spatial distribution of modeled springtime VAI in the
285 southwestern North America for the three cases under both RCPs by 2100. In RCP4.5, the

286 distributions of changes in VAI are similar for the all-factor and fixed-land use cases. Strong
287 enhancements (up to $\sim 2.5 \text{ m}^2 \text{ m}^{-2}$) extend across much of Arizona, especially in the northwestern
288 corner. The model exhibits moderate VAI increases in most of New Mexico and in the forest
289 regions along the coast of northwestern Mexico. We find decreases in modeled VAI (up to ~ -1.6
290 $\text{m}^2 \text{m}^{-2}$) in the southwestern corner of New Mexico, to the east of the coastal forests in Mexico and
291 in the forest regions near the Mexican border connecting with southern Texas. The similarity
292 between the all-factor and fixed land use cases indicates the relatively trivial influence of land use
293 change on vegetation cover in RCP4.5, compared to the effects of climate change and CO₂
294 fertilization. For the fixed-CO₂ case, western New Mexico and northern Mexico show greater
295 decreases in VAI, indicating how CO₂ fertilization in the other two cases offsets the effects of the
296 warmer, drier climate on vegetation in this region. Figure S8 further illustrates the strong positive
297 impacts that CO₂ fertilization has on VAI.

298 Compared to RCP4.5, the RCP8.5 scenario shows larger changes in climate, CO₂
299 concentrations, and land use by 2100 (Figure 1). The net effects of these changes on vegetation
300 are complex. As in RCP4.5, Arizona experiences a strong increase in VAI in the all-factor and
301 fixed-land use cases, but now this increase extends to New Mexico. In contrast to RCP4.5, modeled
302 VAI decreases in the coastal forest areas in northern Mexico in the all-factor case for RCP8.5. In
303 the fixed-land use case, however, the VAI decrease in northern Mexico is nearly erased, indicating
304 the role of vegetation/forest degradation caused by land use practices in this area (Figure S9). For
305 the fixed-CO₂ case for RCP8.5, VAI decreases in nearly all of southwestern North America, except
306 the northeastern corner of Arizona and the northwestern corner of New Mexico.

307 To better understand the changes in VAI, we can examine changes in LAI, which
308 represents the major portion of VAI, for the four dominant plant functional types (PFTs) in this

309 region. For example, decreases in LAI in the fixed-CO₂ case under RCP8.5 are dominated by the
310 loss of temperate broadleaf evergreen (TeBE) and temperate broadleaf summergreen (TeBS)
311 (Figure S10). Temperate needleleaf evergreen (TeNE) shows areas of increase in the northern part
312 and south of Texas in this scenario, while both TeBE and TeBS show increases in northern Arizona
313 and New Mexico. In other areas, TeBS reveals strong decreases, especially in southern Arizona
314 and Mexico. As predicted by previous studies (Bestelmeyer et al., 2018; Edwards et al., 2019), C₃
315 perennial grasses (C₃gr) in this case decrease across a large swath extending from Arizona through
316 Mexico, showing the impacts of warmer temperatures and reduced precipitation, as well as (for
317 Mexico) land use change. Increased fire activity also likely plays a role in the simulated decreases
318 of forest cover and C₃ grasses for RCP8.5 in southern Arizona, where fires together with drought
319 may have affected landscape succession (Williams et al., 2013; Bodner and Robles, 2017). We
320 also investigate trends in LAI for different months in spring from the present day to 2100. We find
321 that the greatest percentage decreases in TeBS and C₃ grasses occur in May, consistent with the
322 largest decreases in precipitation in that month (not shown).

323 In sum, we find that the warmer and drier conditions of the future climate strongly reduce
324 vegetation cover by 2100, especially in RCP8.5. In addition, CO₂ fertilization and land use
325 practices further modify future vegetation, but in opposite ways, as illustrated by Figure S8. Under
326 a warmer climate, higher CO₂ concentrations facilitate vegetation growth everywhere in the
327 southwestern North America, with larger VAI increases occurring over Arizona and New Mexico.
328 Combined changes in anthropogenic land use – including cropland, pasture, and urban area – are
329 greater under RCP8.5 than RCP4.5, with large increases in RCP8.5 across Mexico but only modest
330 changes in Arizona, New Mexico, and Texas (Figure S9). The increases in Mexico result in the
331 fragmentation of forested landscapes and decrease VAI, especially in coastal forest regions and

332 along the border with the United States.

333 **3.2 Spatial variations in spring fine dust emissions**

334 Unlike the widespread changes in VAI, future changes in fine dust emissions are
335 concentrated in a few arid areas, including: 1) the border regions connecting Arizona, New Mexico,
336 and northern Mexico (ANM border), 2) eastern New Mexico, and 3) western Texas (Figure 2). In
337 RCP4.5, slight increases in fine dust emission (up to $\sim 0.3 \text{ kg m}^{-2} \text{ mon}^{-1}$) are simulated in the ANM
338 border in all the three cases. In contrast, fine dust emissions decrease by up to $\sim -1.0 \text{ kg m}^{-2} \text{ mon}^{-1}$
339 ¹ in eastern New Mexico and western Texas in RCP4.5 due to warmer temperatures and increasing
340 VAI. Consistent with the modest changes in VAI (Figure 1), the three cases in RCP4.5 do not
341 exhibit large differences, with only the fixed-CO₂ case showing slightly greater increases in dust
342 emissions along the ANM border and in western Texas. In RCP8.5 in the all-factor case, spring
343 fine dust emissions increase slightly by up to $\sim 0.4 \text{ kg m}^{-2} \text{ mon}^{-1}$ along the ANM border, but
344 decrease more strongly in western Texas by up to $\sim -1.4 \text{ kg m}^{-2} \text{ mon}^{-1}$ (Figure 2). In contrast, with
345 fixed CO₂ the sign of the change in dust emissions reverses, with significant emissions increases
346 along the ANM border and in New Mexico. The area with decreasing emissions in western Texas
347 also shrinks in the fixed CO₂ case. These trends occur due to the climate stresses – e.g., warmer
348 temperatures and decreased precipitation – that impair the growth of temperature broadleaf trees
349 and C₃ grasses. In this case, such stresses are not offset by CO₂ fertilization (Figure S10).

350 Figure 3 shows more vividly the opposing roles of CO₂ fertilization and projected land use
351 change in southwestern North America. In RCP8.5, changing CO₂ fertilization alone promotes
352 vegetation growth and dramatically reduces dust mobilization by up to $\sim -1.2 \text{ kg m}^{-2} \text{ mon}^{-1}$. Figure
353 3 also reveals that land use trends are a major driver of increased dust emissions along the ANM
354 border and western Texas in RCP8.5, as crop- and rangelands expand in this region and

355 temperature broadleaf trees decline (Hurtt et al., 2011). Similarly, the expansion of rangelands in
356 northern Mexico in RCP8.5 reduces natural vegetation cover there (Hurtt et al., 2011), contributing
357 to the increase of fine dust emissions by up to $\sim 0.7 \text{ kg m}^{-2} \text{ mon}^{-1}$.

358 **3.3 Spring fine dust concentrations under the high emission scenario**

359 Our simulations suggest that fine dust emissions will increase across arid areas in
360 southwestern North America under RCP8.5, but only if CO_2 fertilization is of minimal importance
361 (Figure 2). To place an upper bound on future concentrations of fine dust in this region, we apply
362 only the fixed- CO_2 emissions to GEOS-Chem at the horizontal resolution of $0.5^\circ \times 0.625^\circ$. Given
363 the large uncertainty in the sensitivity of vegetation to changing atmospheric CO_2 concentrations
364 (Smith et al., 2016), we argue that this approach is justified.

365 Results from GEOS-Chem in the fixed- CO_2 case for RCP8.5 show that the concentrations
366 of spring fine dust are significantly enhanced in the southeastern half of New Mexico and along
367 the ANM border, with increases up to $\sim 2.5 \mu\text{g m}^{-3}$ (Figure 4). The model also yields elevated dust
368 concentrations over nearly the entire extent of our study region by 2100. As Figure 3 implies,
369 anthropogenic land use along the ANM border contributes to the increased dust emissions in that
370 area, by up to $\sim 0.7 \text{ kg m}^{-2} \text{ mon}^{-1}$. Climate change impacts on natural vegetation, however, account
371 for the bulk of the modeled increases in dust emissions in this scenario, by as much as $\sim 1.2 \text{ kg m}^{-2}$
372 mon^{-1} (Figure 2). The modeled wind fields, which are the same in all scenarios, transport the dust
373 from source regions, leading to the enhanced concentrations across much of the domain, as seen
374 in Figure 4. We find that dust concentrations decrease only in a limited area in western Texas due
375 to decreased pasture (Figures 3 and S9).

376

377 **4 Discussion**

378 We apply a coupled modeling approach to investigate the impact of future changes in
379 climate, CO₂ fertilization, and anthropogenic land use on dust mobilization and fine dust
380 concentration in southwestern North America by the end of the 21st century. Table 1 summarizes
381 our findings for the two RCP scenarios and three conditions – all-factor, fixed CO₂, and fixed land
382 use – in spring, when dust concentrations are greatest. We find that in the RCP8.5 fixed-CO₂
383 scenario, in which the effects of CO₂ fertilization are neglected, VAI decreases by 26% across the
384 region due mainly to warmer temperatures and drier conditions, yielding an increase of 58% in
385 fine dust emission averaged over the southwestern North America. In addition, we find that the
386 increase in fine dust emission in northern Mexico is mainly driven by the increases in the extent
387 of cropland and pasture cover in this area, signifying the crucial role of land use practices in
388 modifying dust mobilization.

389 Our findings for diminished VAI in the future atmosphere are consistent with observed
390 trends in vegetation during recent droughts in this region. For example, Breshears et al., 2005
391 documented large-scale die-off of overstory trees across southwestern North America in 2002-
392 2003 in response to short-term drought accompanied by bark beetle infestations. Similarly, during
393 a multi-year (2004-2014) drought in southern Arizona, Bodner and Robles, 2017 found that the
394 spatial extent of both C₄ grass cover and shrub cover decreased in the southeast part of that state.

395 The 58% increase predicted in this study in fixed-CO₂ RCP8.5 scenario is larger than the
396 26-46% future increases in fine dust for this region predicted by the statistical model of
397 Achakulwisut et al., 2018. That study relied solely on predictions of future regional-scale
398 meteorology and did not take into account the change in vegetation, as we do here. In contrast, the
399 statistical model of Pu and Ginoux, 2017 estimated a 2% decrease in the springtime frequency of
400 extreme dust events in the Southwest U.S., driven mainly by reductions in bare ground fraction

401 and wind speed. Like Pu and Ginoux, 2017, we also find that dust emissions decrease across a
402 broad region of the Southwest when CO₂ fertilization is taken into account, as shown in Figure 2.
403 Pu and Ginoux, 2017 relied on limited data for capturing the sensitivity of dust event frequency to
404 land cover in this region, and neither that study nor Achakulwisut et al., 2018 considered changes
405 in land use, as do here. The direct effects of changing wind speed on dust mobilization, however,
406 are not included in our study, but could be tested in future work.

407 We further find that consideration of CO₂ fertilization can mitigate the effects of changing
408 climate and land use on dust concentrations in southwestern North America. The all-factor and
409 fixed-land use simulations both yield decreases of ~20% in mean dust emissions compared to the
410 early 21st century. In the IPCC projections, CO₂ reaches ~550 ppm by 2100 under RCP4.5 and
411 ~1960 ppm under RCP8.5 (Meinshausen et al., 2011). Correspondingly, in the RCP4.5 scenario
412 for 2100, CO₂ fertilization enhances VAI by 30% in the all-factor case compared to the fixed-CO₂
413 case (1.07 m²m⁻² vs. 0.79 m²m⁻²) ; in RCP 8.5, the 2100 enhancement is 64% (1.11 m²m⁻² vs. 0.55
414 m²m⁻²), as shown in Table 1. These enhancements further decrease fine dust emissions by 21%
415 under RCP4.5 and 78% under RCP8.5, compared to the present day. Except along the ANM border
416 and a few other areas, trends in land use have only minor impacts on dust mobilization under the
417 two RCPs in southwestern North America.

418 In sum, we find that as atmospheric CO₂ levels rise, the effect of enhanced CO₂ fertilization
419 boosts vegetation growth and decreases dust mobilization, offsetting the impacts of warmer
420 temperatures and reduced rainfall, at least in some areas. These results are consistent with evidence
421 that enhanced CO₂ fertilization is already occurring in arid or semiarid environments like
422 southwestern North America (Donohue et al., 2013; Haverd et al., 2020). In such environments,
423 water availability is the dominant constraint on vegetation growth, and the recent enhancement of

424 atmospheric CO₂ may have reduced stomatal conductance and limited evaporative water loss. The
425 effects of CO₂ fertilization on vegetation growth are uncertain, however, and may be attenuated
426 by the limited supply of nitrogen and phosphorus in soil (Wieder et al., 2015). These nutritional
427 constraints vary greatly among different PFTs (Shaw et al., 2002; Nadelhoffer et al., 1999).

428 Understanding the drivers in historic dust trends has sometimes been challenging
429 (Mahowald and Luo, 2003; Mahowald et al., 2002), making it difficult to validate dust
430 mobilization models. A further drawback of our approach is that the LPJ-LMfire model is driven
431 by meteorological fields from just one climate model, GISS-E2-R. Given that the GISS model
432 yields a conservative prediction of climate change in the southwestern North America compared
433 to other models (Ahlström et al., 2012; Sheffield et al., 2013), our predictions of the impact of
434 climate change on dust mobilization may also be conservative. Other uncertainties in our study
435 can be traced to the dust simulation. The different vegetation types in our model are quantified as
436 fractions of gridcells, which have relatively large spatial dimensions of ~50 km × 60 km. This
437 means the model cannot capture the spatial heterogeneity of land cover, and the aerodynamic
438 sheltering effects of vegetation on wind erosion are neglected, as they are in most 3-D global model
439 studies. Such sheltering could play a large role in dust mobilization (e.g., Liu et al., 1990). New
440 methods involving satellite observations of surface albedo promise to improve understanding of
441 the effects of aerodynamic sheltering on dust mobilization, at least for the present-day (Chappell
442 and Webb, 2016; Webb and Pierre, 2018). Implementation of aerodynamic sheltering in
443 simulations of future climate regimes would need to account for fine-scale spatial distributions of
444 vegetation. In addition, as recommended by Zender et al., 2003, we apply a globally uniform
445 surface roughness Z_0 in the model, which means that the impact of changing vegetation conditions
446 on friction velocity is not taken into account. Future work could address this weakness by varying

447 friction velocity according to vegetation type. Finally, our study focuses only on the effect of
448 changing vegetation on dust mobilization and does not take into account how changing windspeeds
449 or drier soils in the future atmosphere may more directly influence dust. Given the slight increase
450 in monthly mean winds in RCP8.5 by 2100, future dust emissions in this scenario could be
451 underestimated.

452 Within these limitations, our study quantifies the potential impacts of changing land cover
453 and land use practices on dust mobilization and fine dust concentration over the coming century
454 in southwestern North America. Our work builds on previous studies focused on future dust in this
455 region by (1) more accurately capturing the transport of dust from source regions with a dynamical
456 3-D model, (2) considering results with and without CO₂ enhancement, and (3) including the
457 impact of land use trends. Given the many uncertainties, it is challenging to gauge which of the
458 three factors investigated here – climate impacts on vegetation, CO₂ fertilization, or land use
459 change – will play the dominant role in driving future changes in dust emissions and concentrations.
460 This study thus brackets a range of possible dust scenarios for the southwestern North America,
461 with the simulation without CO₂ fertilization placing an upper bound on dust emissions. In the
462 absence of increased CO₂ fertilization, our work suggests that vegetated area will contract in
463 response to the warmer, drier climate, exposing bare land and significantly increasing dust
464 concentrations by 2100.

465 Dust enhancement could thus impose a potentially large climate penalty on PM_{2.5} air
466 quality, with consequences for human health across much of southwestern North America, where
467 much of the current population is of Native American and/or Latino descent. In New Mexico for
468 example, 10% of the population is Native American and 50% identifies as either Hispanic or Latino.
469 By some measures, New Mexico has also one of highest poverty rates of the United States

470 (<https://www.census.gov/quickfacts/NM>, last accessed on August 20, 2020). In this way, our
471 finding of the potential for an increased dust burden in the future atmosphere has special relevance
472 for environmental justice in this region.

473

474 **Code and data availability**

475 GEOS-Chem model codes can be obtained at <http://acmg.seas.harvard.edu/geos>. LPJ-LMfire
476 model codes can be obtained at <https://github.com/ARVE-Research/LPJ-LMfire>. IMPROVE
477 datasets are available online at <http://vista.cira.colostate.edu/improve>. Any additional information
478 related to this paper may be requested from the authors.

479

480 **Author contributions**

481 Y.L. conceived and designed the study, performed the GEOS-Chem simulations, analyzed the data,
482 and wrote the manuscript, with contributions from all coauthors. J.O.K. performed the LPJ-LMfire
483 simulations.

484

485 **Competing interests**

486 The authors declare that they have no competing interest.

487

488 **Acknowledgments**

489 This research was developed under Assistance Agreements 83587501 and 83587201 awarded by
490 the U.S. Environmental Protection Agency (EPA). It has not been formally reviewed by the EPA.
491 The views expressed in this document are solely those of the authors and do not necessarily reflect
492 those of the EPA. We thank all of the data providers of the datasets used in this study. PM data
493 was provided by the Interagency Monitoring of Protected Visual Environments (IMPROVE;
494 available online at <http://vista.cira.colostate.edu/improve>). IMPROVE is a collaborative
495 association of state, tribal, and federal agencies, and international partners. U.S. Environmental
496 Protection Agency is the primary funding source, with contracting and research support from the
497 National Park Service. JOK is grateful for access to computing resources provided by the School
498 of Geography and the Environment, University of Oxford. The Air Quality Group at the University
499 of California, Davis is the central analytical laboratory, with ion analysis provided by the Research
500 Triangle Institute, and carbon analysis provided by the Desert Research Institute. We acknowledge
501 the World Climate Research Programme's Working Group on Coupled Modelling, which is
502 responsible for CMIP, and we thank the group of NASA Goddard Institute for Space Studies for
503 producing and making available their GISS-E2-R climate model output. For CMIP the U.S.
504 Department of Energy's Program for Climate Model Diagnosis and Intercomparison provides
505 coordinating support and led development of software infrastructure in partnership with the Global
506 Organization for Earth System Science Portals. The GISS-E2-R dataset were downloaded from
507 <https://cmip.llnl.gov/cmip5/>. We thank the Land-use Harmonization team for producing the
508 harmonized set of land-use scenarios and making available the dataset online at
509 <http://tntcat.iiasa.ac.at/RcpDb/>. We also thank the founder, organizers, and participants of the
510 Degree Confluence Project (www.confluence.org).

511 **References**

- 512 Achakulwisut, P., Shen, L., and Mickley, L. J.: What controls springtime fine dust variability in
513 the western United States? Investigating the 2002–2015 increase in fine dust in the US
514 Southwest, *Journal of Geophysical Research: Atmospheres*, 122, 2017.
- 515 Achakulwisut, P., Mickley, L., and Anenberg, S.: Drought-sensitivity of fine dust in the US
516 Southwest: Implications for air quality and public health under future climate change,
517 *Environmental Research Letters*, 13, 054025, 2018.
- 518 Ahlström, A., Schurgers, G., Arneth, A., and Smith, B.: Robustness and uncertainty in terrestrial
519 ecosystem carbon response to CMIP5 climate change projections, *Environmental Research*
520 *Letters*, 7, 044008, 2012.
- 521 Andreadis, K. M., Clark, E. A., Wood, A. W., Hamlet, A. F., and Lettenmaier, D. P.: Twentieth-
522 century drought in the conterminous United States, *Journal of Hydrometeorology*, 6, 985-1001,
523 2005.
- 524 Archer, S. R., and Predick, K. I.: Climate change and ecosystems of the southwestern United
525 States, *Rangelands*, 30, 23-28, 2008.
- 526 Belnap, J., and Gillette, D. A.: Vulnerability of desert biological soil crusts to wind erosion: the
527 influences of crust development, soil texture, and disturbance, *Journal of arid environments*,
528 39, 133-142, 1998.
- 529 Bestelmeyer, B. T., Peters, D. P. C., Archer, S. R., Browning, D. M., Okin, G. S., Schooley, R.
530 L., and Webb, N. P.: The Grassland–Shrubland Regime Shift in the Southwestern United
531 States: Misconceptions and Their Implications for Management, *BioScience*, 68, 678-690,
532 10.1093/biosci/biy065, 2018.
- 533 Bodner, G. S., and Robles, M. D.: Enduring a decade of drought: Patterns and drivers of
534 vegetation change in a semi-arid grassland, *Journal of Arid Environments*, 136, 1-14, 2017.
- 535 Breshears, D. D., Cobb, N. S., Rich, P. M., Price, K. P., Allen, C. D., Balice, R. G., Romme, W.
536 H., Kastens, J. H., Floyd, M. L., Belnap, J., Anderson, J. J., Myers, O. B., and Meyer, C. W.:
537 Regional vegetation die-off in response to global-change-type drought, *Proc Natl Acad Sci U S*
538 *A*, 102, 15144-15148, 10.1073/pnas.0505734102, 2005.
- 539 Chappell, A., and Webb, N. P.: Using albedo to reform wind erosion modelling, mapping and
540 monitoring, *Aeolian Research*, 23, 63-78, 2016.
- 541 Chaste, E., Girardin, M. P., Kaplan, J. O., Bergeron, Y., and Hély, C.: Increases in heat-induced
542 tree mortality could drive reductions of biomass resources in Canada’s managed boreal forest,
543 *Landscape Ecology*, 34, 403-426, 2019.
- 544 Donohue, R. J., Roderick, M. L., McVicar, T. R., and Farquhar, G. D.: Impact of CO₂
545 fertilization on maximum foliage cover across the globe's warm, arid environments,
546 *Geophysical Research Letters*, 40, 3031-3035, 2013.
- 547 Edwards, B., Webb, N., Brown, D., Elias, E., Peck, D., Pierson, F., Williams, C., and Herrick, J.:
548 Climate change impacts on wind and water erosion on US rangelands, *Journal of Soil and*
549 *Water Conservation*, 74, 405-418, 2019.
- 550 Fairlie, T. D., Jacob, D. J., and Park, R. J.: The impact of transpacific transport of mineral dust in
551 the United States, *Atmos Environ*, 41, 1251-1266, 2007.
- 552 Gelaro, R., McCarty, W., Suarez, M. J., Todling, R., Molod, A., Takacs, L., Randles, C.,
553 Darmenov, A., Bosilovich, M. G., Reichle, R., Wargan, K., Coy, L., Cullather, R., Draper, C.,
554 Akella, S., Buchard, V., Conaty, A., da Silva, A., Gu, W., Kim, G. K., Koster, R., Lucchesi, R.,
555 Merkova, D., Nielsen, J. E., Partyka, G., Pawson, S., Putman, W., Rienecker, M., Schubert, S.

556 D., Sienkiewicz, M., and Zhao, B.: The Modern-Era Retrospective Analysis for Research and
557 Applications, Version 2 (MERRA-2), *J Clim*, Volume 30, 5419-5454, 10.1175/JCLI-D-16-
558 0758.1, 2017.

559 Goldewijk, K. K.: Estimating global land use change over the past 300 years: the HYDE
560 database, *Global biogeochemical cycles*, 15, 417-433, 2001.

561 Goldewijk, K. K., Beusen, A., van Drecht, G., and de Vos, M.: The HYDE 3.1 spatially explicit
562 database of human-induced global land-use change over the past 12,000 yearsgeb_587, 2010.

563 Gorris, M. E., Cat, L. A., Zender, C. S., Treseder, K. K., and Randerson, J. T.:
564 Coccidioidomycosis Dynamics in Relation to Climate in the Southwestern United States,
565 *Geohealth*, 2, 6-24, 10.1002/2017GH000095, 2018.

566 Hand, J., White, W., Gebhart, K., Hyslop, N., Gill, T., and Schichtel, B.: Earlier onset of the
567 spring fine dust season in the southwestern United States, *Geophysical Research Letters*, 43,
568 4001-4009, 2016.

569 Hand, J., Gill, T., and Schichtel, B.: Spatial and seasonal variability in fine mineral dust and
570 coarse aerosol mass at remote sites across the United States, *Journal of Geophysical Research:*
571 *Atmospheres*, 122, 3080-3097, 2017.

572 Harrison, S. P., Kohfeld, K. E., Roelandt, C., and Claquin, T.: The role of dust in climate
573 changes today, at the last glacial maximum and in the future, *Earth-Science Reviews*, 54, 43-
574 80, 2001.

575 Haverd, V., Smith, B., Canadell, J. G., Cuntz, M., Mikaloff-Fletcher, S., Farquhar, G.,
576 Woodgate, W., Briggs, P. R., and Trudinger, C. M.: Higher than expected CO2 fertilization
577 inferred from leaf to global observations, *Global change biology*, 26, 2390-2402, 2020.

578 Hillel, D.: *Introduction to soil physics.*(Academic Press: San Diego, CA), *Introduction to soil*
579 *physics.* Academic Press, San Diego, CA., -, 1982.

580 Hurtt, G. C., Chini, L. P., Frolking, S., Betts, R., Feddema, J., Fischer, G., Fisk, J., Hibbard, K.,
581 Houghton, R., and Janetos, A.: Harmonization of land-use scenarios for the period 1500–2100:
582 600 years of global gridded annual land-use transitions, wood harvest, and resulting secondary
583 lands, *Climatic change*, 109, 117, 2011.

584 Li, Y., Mickley, L. J., Liu, P., and Kaplan, J. O.: Trends and spatial shifts in lightning fires and
585 smoke concentrations in response to 21st century climate over the national forests and parks of
586 the western United States, *Atmospheric Chemistry and Physics*, 20, 8827-8838, 10.5194/acp-
587 20-8827-2020, 2020.

588 Liu, S.-J., Wu, H.-I., Lytton, R. L., and Sharpe, P. J.: Aerodynamic sheltering effects of
589 vegetative arrays on wind erosion: A numerical approach, *Journal of environmental*
590 *management*, 30, 281-294, 1990.

591 MacDonald, G. M.: Climate Change and water in Southwestern North America special feature:
592 water, climate change, and sustainability in the southwest, *Proc Natl Acad Sci U S A*, 107,
593 21256-21262, 10.1073/pnas.0909651107, 2010.

594 Magi, B. I.: Global lightning parameterization from CMIP5 climate model output, *Journal of*
595 *Atmospheric and Oceanic Technology*, 32, 434-452, 2015.

596 Mahowald, N., Kohfeld, K., Hansson, M., Balkanski, Y., Harrison, S. P., Prentice, I. C., Schulz,
597 M., and Rodhe, H.: Dust sources and deposition during the last glacial maximum and current
598 climate: A comparison of model results with paleodata from ice cores and marine sediments,
599 *Journal of Geophysical Research: Atmospheres*, 104, 15895-15916, 1999.

600 Mahowald, N. M., Zender, C. S., Luo, C., Savoie, D., Torres, O., and Del Corral, J.:
601 Understanding the 30-year Barbados desert dust record, *Journal of Geophysical Research:*
602 *Atmospheres*, 107, AAC 7-1-AAC 7-16, 2002.

603 Mahowald, N. M., and Luo, C.: A less dusty future?, *Geophysical Research Letters*, 30, 2003.

604 Mahowald, N. M., Muhs, D. R., Levis, S., Rasch, P. J., Yoshioka, M., Zender, C. S., and Luo, C.:
605 Change in atmospheric mineral aerosols in response to climate: Last glacial period,
606 preindustrial, modern, and doubled carbon dioxide climates, *Journal of Geophysical Research:*
607 *Atmospheres*, 111, 2006.

608 McClaran, M. P., and Van Devender, T. R.: *The desert grassland*, University of Arizona Press,
609 1997.

610 Meinshausen, M., Smith, S. J., Calvin, K., Daniel, J. S., Kainuma, M., Lamarque, J.-F.,
611 Matsumoto, K., Montzka, S., Raper, S., and Riahi, K.: The RCP greenhouse gas concentrations
612 and their extensions from 1765 to 2300, *Climatic change*, 109, 213, 2011.

613 Meng, Z., and Lu, B.: Dust events as a risk factor for daily hospitalization for respiratory and
614 cardiovascular diseases in Minqin, China, *Atmos Environ*, 41, 7048-7058, 2007.

615 Nadelhoffer, K. J., Emmett, B. A., Gundersen, P., Kjønaas, O. J., Koopmans, C. J., Schleppi, P.,
616 Tietema, A., and Wright, R. F.: Nitrogen deposition makes a minor contribution to carbon
617 sequestration in temperate forests, *Nature*, 398, 145, 1999.

618 Nazarenko, L., Schmidt, G., Miller, R., Tausnev, N., Kelley, M., Ruedy, R., Russell, G., Aleinov,
619 I., Bauer, M., and Bauer, S.: Future climate change under RCP emission scenarios with GISS
620 ModelE2, *Journal of Advances in Modeling Earth Systems*, 7, 244-267, 2015.

621 Nicholson, S. E., Tucker, C. J., and Ba, M.: Desertification, drought, and surface vegetation: An
622 example from the West African Sahel, *Bulletin of the American Meteorological Society*, 79,
623 815-830, 1998.

624 Park, R. J., Jacob, D. J., Field, B. D., Yantosca, R. M., and Chin, M.: Natural and transboundary
625 pollution influences on sulfate-nitrate-ammonium aerosols in the United States: Implications
626 for policy, *Journal of Geophysical Research: Atmospheres*, 109, 2004.

627 Pfeiffer, M., Spessa, A., and Kaplan, J. O.: A model for global biomass burning in preindustrial
628 time: LPJ-LMfire (v1. 0), *Geoscientific Model Development*, 6, 643-685, 2013.

629 Polley, H. W., Briske, D. D., Morgan, J. A., Wolter, K., Bailey, D. W., and Brown, J. R.: Climate
630 change and North American rangelands: trends, projections, and implications, *Rangeland*
631 *Ecology & Management*, 66, 493-511, 2013.

632 Poorter, H., and Perez-Soba, M.: Plant growth at elevated CO₂, *Encyclopedia of global*
633 *environmental change*, 2, 489-496, 2002.

634 Prein, A. F., Holland, G. J., Rasmussen, R. M., Clark, M. P., and Tye, M. R.: Running dry: The
635 US Southwest's drift into a drier climate state, *Geophysical Research Letters*, 43, 1272-1279,
636 2016.

637 Pu, B., and Ginoux, P.: Projection of American dustiness in the late 21(st) century due to climate
638 change, *Sci Rep*, 7, 5553, 10.1038/s41598-017-05431-9, 2017.

639 Raupach, M.: Simplified expressions for vegetation roughness length and zero-plane
640 displacement as functions of canopy height and area index, *Boundary-Layer Meteorol*, 71, 211-
641 216, 1994.

642 Ridley, D. A., Heald, C. L., Pierce, J., and Evans, M.: Toward resolution-independent dust
643 emissions in global models: Impacts on the seasonal and spatial distribution of dust,
644 *Geophysical Research Letters*, 40, 2873-2877, 2013.

645 Seager, R., and Vecchi, G. A.: Greenhouse warming and the 21st century hydroclimate of
646 southwestern North America, *Proc Natl Acad Sci U S A*, 107, 21277-21282,
647 10.1073/pnas.0910856107, 2010.

648 Shaw, M. R., Zavaleta, E. S., Chiariello, N. R., Cleland, E. E., Mooney, H. A., and Field, C. B.:
649 Grassland responses to global environmental changes suppressed by elevated CO₂, *Science*,
650 298, 1987-1990, 10.1126/science.1075312, 2002.

651 Sheffield, J., Barrett, A. P., Colle, B., Nelun Fernando, D., Fu, R., Geil, K. L., Hu, Q., Kinter, J.,
652 Kumar, S., and Langenbrunner, B.: North American climate in CMIP5 experiments. Part I:
653 Evaluation of historical simulations of continental and regional climatology, *Journal of*
654 *Climate*, 26, 9209-9245, 2013.

655 Sitch, S., Smith, B., Prentice, I. C., Arneth, A., Bondeau, A., Cramer, W., Kaplan, J. O., Levis,
656 S., Lucht, W., Sykes, M. T., Thonicke, K., and Venevsky, S.: Evaluation of ecosystem
657 dynamics, plant geography and terrestrial carbon cycling in the LPJ dynamic global vegetation
658 model, *Global Change Biology*, 9, 161-185, 10.1046/j.1365-2486.2003.00569.x, 2003.

659 Smith, W. K., Reed, S. C., Cleveland, C. C., Ballantyne, A. P., Anderegg, W. R., Wieder, W. R.,
660 Liu, Y. Y., and Running, S. W.: Large divergence of satellite and Earth system model
661 estimates of global terrestrial CO₂ fertilization, *Nature Climate Change*, 6, 306, 2016.

662 Stahle, D. W.: Anthropogenic megadrought, *Science*, 368, 238-239, 10.1126/science.abb6902,
663 2020.

664 Tegen, I., Werner, M., Harrison, S., and Kohfeld, K.: Relative importance of climate and land
665 use in determining present and future global soil dust emission, *Geophysical Research Letters*,
666 31, 2004.

667 Tong, D. Q., Wang, J. X. L., Gill, T. E., Lei, H., and Wang, B.: Intensified dust storm activity
668 and Valley fever infection in the southwestern United States, *Geophys Res Lett*, 44, 4304-
669 4312, 10.1002/2017GL073524, 2017.

670 Van Loon, A. F., Stahl, K., Di Baldassarre, G., Clark, J., Rangelcroft, S., Wanders, N., Gleeson,
671 T., Van Dijk, A. I., Tallaksen, L. M., and Hannaford, J.: Drought in a human-modified world:
672 reframing drought definitions, understanding, and analysis approaches, 2016.

673 Webb, N. P., and Pierre, C.: Quantifying anthropogenic dust emissions, *Earth's Future*, 6, 286-
674 295, 2018.

675 Wieder, W. R., Cleveland, C. C., Smith, W. K., and Todd-Brown, K.: Future productivity and
676 carbon storage limited by terrestrial nutrient availability, *Nature Geoscience*, 8, 441, 2015.

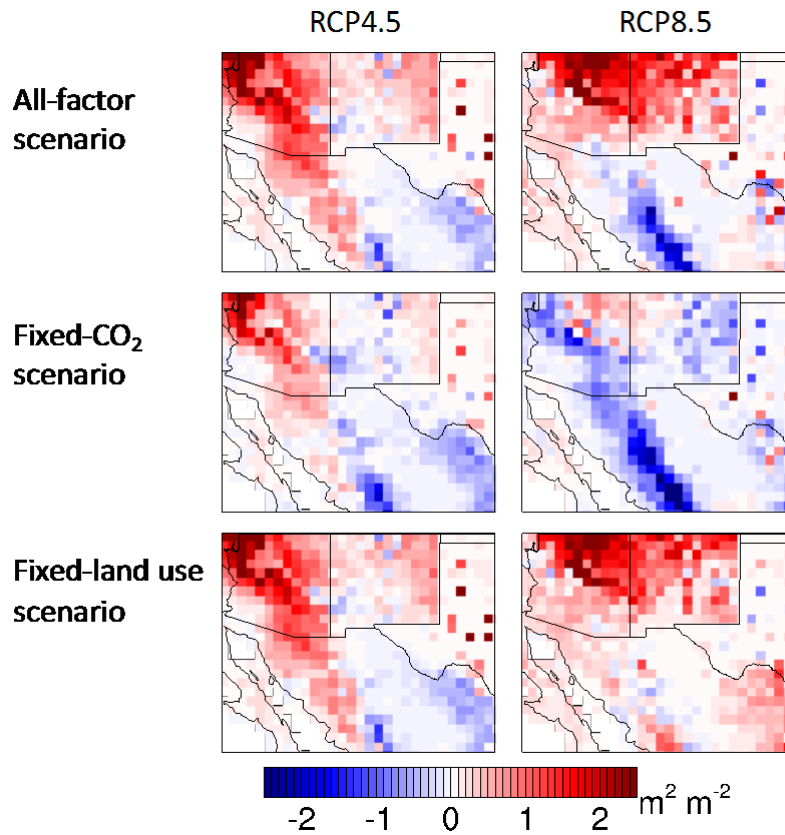
677 Williams, A. P., Allen, C. D., Macalady, A. K., Griffin, D., Woodhouse, C. A., Meko, D. M.,
678 Swetnam, T. W., Rauscher, S. A., Seager, R., and Grissino-Mayer, H. D.: Temperature as a
679 potent driver of regional forest drought stress and tree mortality, *Nature climate change*, 3,
680 292-297, 2013.

681 Williams, A. P., Cook, E. R., Smerdon, J. E., Cook, B. I., Abatzoglou, J. T., Bolles, K., Baek, S.
682 H., Badger, A. M., and Livneh, B.: Large contribution from anthropogenic warming to an
683 emerging North American megadrought, *Science*, 368, 314-318, 2020.

684 Woodward, S., Roberts, D., and Betts, R.: A simulation of the effect of climate change-induced
685 desertification on mineral dust aerosol, *Geophysical Research Letters*, 32, 2005.

686 Zender, C. S., Bian, H., and Newman, D.: Mineral Dust Entrainment and Deposition (DEAD)
687 model: Description and 1990s dust climatology, *Journal of Geophysical Research:*
688 *Atmospheres*, 108, 2003.

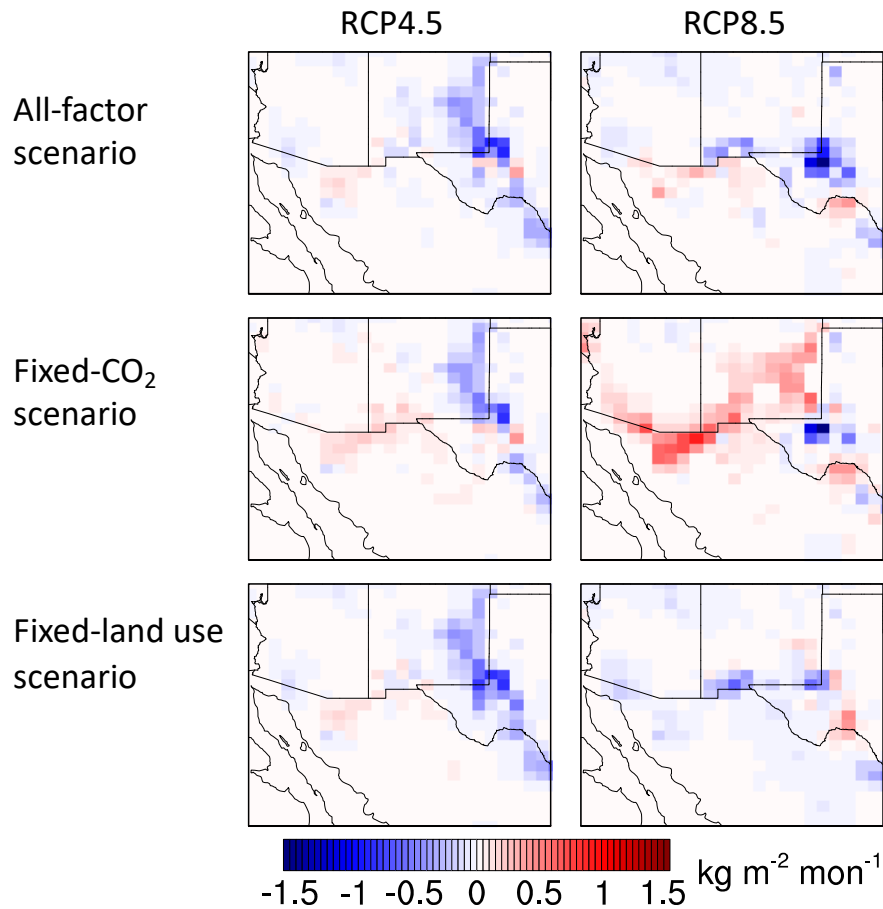
689 Zeng, X., Shaikh, M., Dai, Y., Dickinson, R. E., and Myneni, R.: Coupling of the common land
690 model to the NCAR community climate model, *Journal of Climate*, 15, 1832-1854, 2002.



693

694 **Figure 1.** Simulated changes in spring averaged monthly mean vegetation area index (VAI) in
 695 southwestern North America under the three conditions for RCP4.5 and RCP8.5. Changes are
 696 between the present day and 2100, with five years representing each time period. The All-factor
 697 case (top row) includes the effects of climate, CO₂ fertilization, and anthropogenic land use on
 698 vegetation. Only climate and land use are considered in the Fixed-CO₂ case (middle), and only
 699 climate and CO₂ fertilization are considered in the Fixed-land use case (bottom). Results are from
 700 LPJ-LMfire.

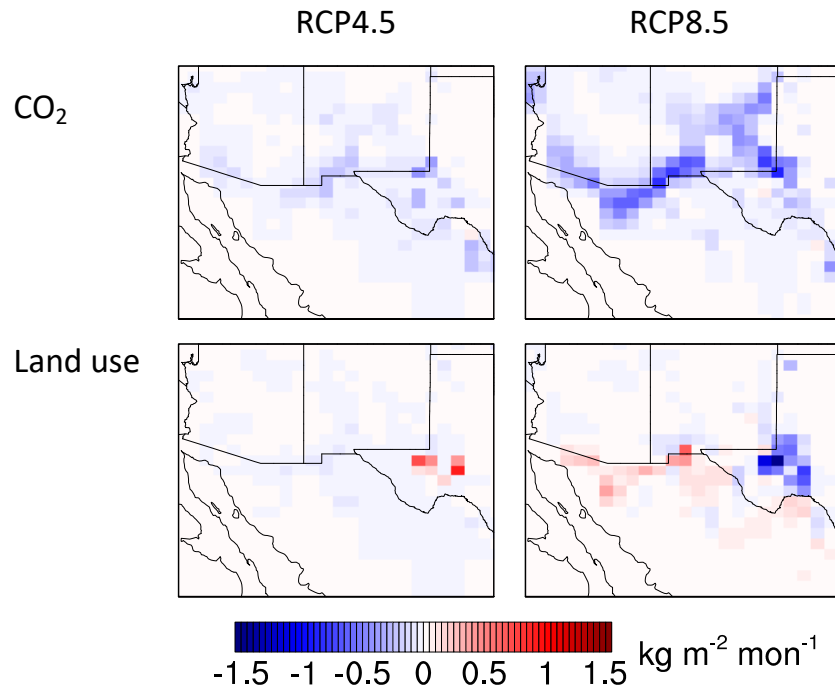
701



702

703 **Figure 2.** Simulated changes in spring averaged monthly mean dust emission in southwestern
 704 North America under the three conditions for RCP4.5 and RCP8.5. Changes are between the
 705 present day and 2100, with five years representing each time period. The top row shows results for
 706 the all-factor condition, the middle row is for the fixed-CO₂ condition, and the bottom row is for
 707 the fixed-land use condition. Cases are as described in Figure 1. Results are generated offline using
 708 the GEOS-Chem emission component (HEMCO).

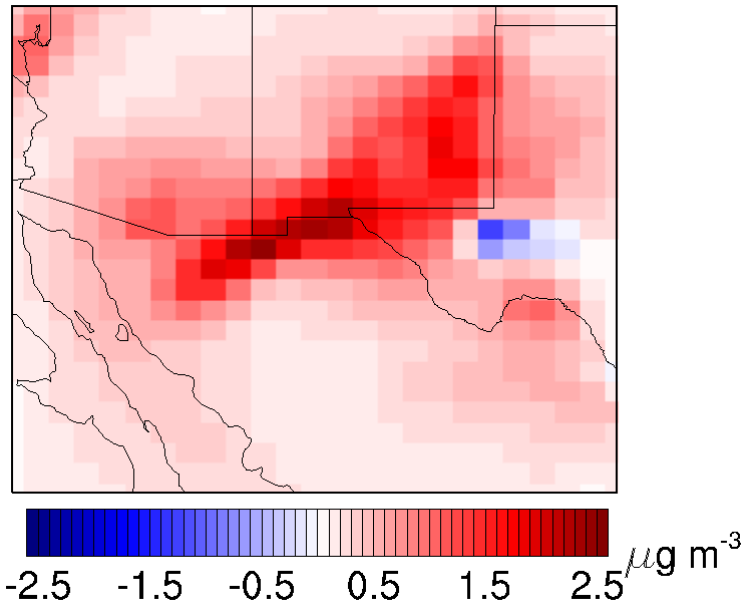
709



710

711 **Figure 3.** Contributions of CO₂ fertilization and land use change to changing dust emissions in
 712 spring in southwestern North America for RCP4.5 and RCP8.5. Changes are between the present
 713 day and 2100, with five years representing each time period. The top row shows the response of
 714 dust emission to only CO₂ fertilization and the bottom row shows the response to only trends in
 715 land use. Results are generated offline using the GEOS-Chem emission component (HEMCO).

716



717

718 **Figure 4.** Simulated changes in springtime mean concentrations of fine dust over southwestern
 719 North America for the RCP8.5 fixed-CO₂ case, in which the effects of CO₂ fertilization are
 720 neglected. Changes are between the present day and 2100, with five years representing each time
 721 period. Results are from GEOS-Chem simulations at 0.5° x 0.625° resolution.

722

723 **Table 1.** Averaged spring vegetation area index (VAI) and fine dust emission in southwestern
724 North America for the present-day and future for two scenarios (RCP4.5 and RCP8.5) and three
725 cases. The all-factor case includes changes in climate, land use, and CO₂ fertilization; the fixed-
726 CO₂ case includes changes in only climate and land use; and the fixed-land use case includes
727 changes in only climate and CO₂. The rows labeled “2100-2010, %” give the percentage changes
728 in VAI and fine dust emissions between the present day and future, with positive values denoting
729 increases in the future.

		VAI ^b , m ² m ⁻²			Fine dust emission ^b , kg m ⁻² mon ⁻¹		
		All-factor	Fixed CO ₂	Fixed land use	All-factor	Fixed CO ₂	Fixed land use
RCP4.5	2010^a	0.75±0.26	0.71±0.24	0.75±0.26	0.10±0.07	0.11±0.08	0.10±0.07
	2100^a	1.07±0.48	0.79±0.34	1.07±0.48	0.08±0.04	0.10±0.05	0.08±0.04
2100-2010, %		42	12	42	-25	-4	-26
RCP8.5	2010^a	0.80±0.27	0.75±0.24	0.75±0.24	0.09±0.04	0.09±0.05	0.09±0.04
	2100^a	1.11±0.71	0.55±0.33	0.55±0.33	0.07±0.04	0.14±0.09	0.07±0.06
2100-2010, %		38	-26	52	-20	58	-16

730 ^aEach time slice represents 5 years (i.e., 2011-2015 represents the 2010 time slice and 2095-2099 represents the 2100
731 time slice); ^bValues are spring (MAM) averages over southwestern North America.